From biomass-derived fructose to γ-valerolactone: Process design and techno-economic assessment

Daniele Di Menno Di Bucchianico, Giordano Emrys Scarponi, Jean-Christophe Buvat, Sébastien Leveneur, Valeria Casson Moreno

From biomass-derived fructose to γ-valerolactone: process design and techno-economic assessment

Abstract

This work proposes a process design and techno-economic assessment for the production of γ-valerolactone from lignocellulosic derived fructose at industrial scale, with the aim of exploring its feasibility, identifying potential obstacles, and suggesting improvements in the context of France.
First, the conceptual process design is developed, the process modelled and optimized. Second, different potential scenarios for the energy supply to the process are analyzed by means of a set of economic key performance indicators, aimed at highlighting the best potential profitability scenario for the sustainable exploitation of waste biomass in the context analyzed. The lowest Minimum Selling Price for GVL is obtained at 10 kt/y plant fueled by biomass, i.e. 1.89 €/kg, along with the highest end-of-live revenue, i.e. 113 M€. Finally, a sensitivity and uncertainties analysis, based on Monte Carlo simulations, are carried out on the results in order to test their robustness with respect to key input parameters.

Keywords

gamma valerolactone; fructose; process design; techno-economic assessment; sensitivity analysis;

1. Introduction

Meeting the European 'Carbon Neutrality' targets (NZE2050) (IEA, 2021) requires a drastic transformation of the existing economy, shifting from fossil to renewable alternatives for energy, fuel, and chemical production. Despite the substantial increase in investments towards exploiting renewable resources (RES), currently**,** the industrial and energy sectors remain significantly reliant on fossil fuels. In fact, fossil resources continue to account for over 80% of global energy production (EI, 2023). Using renewable energy resources in combination with CO_2 capture and storage strategies (CCS) is the best option to reduce emissions (Mogoș et al., 2023).
Among the RES, lignocellulosic biomass (LCB) stands out as the only carbon-fixing resource. LCB is abundant, widespread and provides 55% of the actual renewable energy (6% of total energy supply) (EI, 2023); furthermore, LCB can be used to produce biofuels, solvents, polymers, and additives, to improve hard-to-abate sectors such as chemical, petrochemical, transportation, and aviation (Ashokkumar et al., 2022). The potential of LCB depends upon the constituent bio-polymers, i.e. cellulose, hemicellulose, and lignin, and the abundance of hexose and pentose sugar monomers. These components can be converted into high-value molecules through different chemical pathways (Di Menno Di Bucchianico et al., 2021). Among all, a promising route for the conversion of hexose sugars involves acidic solvolysis, in aqueous or organic environment, by homogeneous or heterogeneous Brønsted acid catalysts for the production of a wide range of high added-value products, such as 5-(hydroxymethyl)furfural (5-HMF), furfural (F), levulinic acid (LA), and alkyl levulinates (ALs) (Ashokkumar et al., 2022; Di Menno Di Bucchianico et al., 2021; Tian et al., 2021).

Esters of LA, i.e. ALSs are versatile, high added-value molecules that are suitable as additives for gasoline and diesel, due to their similarity in properties to the fatty acid methyl esters (FAME) of biodiesel (Christensen et al., 2011). Furthermore, high-chain ALs, such as butyl levulinate (BL), are interesting due to their ability to improve the cold flow, conductivity and lubricity properties of diesel, along with reducing its vapor pressure (Alamgir Ahmad et al., 2022; Christensen et al., 2011); in addition, BL has a higher calorific value and cetane number, and a higher compatibility with elastomers, being less corrosive (Alamgir Ahmad et al., 2022; Christensen et al., 2011). Several studies investigates BL potential as a starting molecule for the production of γ-valerolactone (GVL) by hydrogenation on heterogeneous catalyst-based on noble metals, such as ruthenium, which has high selectivity to GVL (Delgado et al., 2022; Ding et al., 2022).

GVL is a promising, safe, and stable bio-solvent for laboratory and large-scale uses, thanks its high polarity (which ensures total miscibility with water and other media (Kerkel et al., 2021)), low volatility (which allows its flammability to be neglected under normal conditions), high thermal stability (Wong et al., 2017), high biodegradability, and low toxicity (Dutta et al., 2020). In addition to its innumerable applications in the cosmetics, pharmaceutical, food and fuel industries (Kerkel et al., 2021), GVL's nature as aprotic and polar, makes it a key solvent in the pre-treatment, fractionation, and processing of LCB (Dutta et al., 2020; Raj et al., 2021), as reported in several studies on the use of GVL to enhance the solubilization and recovery of sugars from LCB (Shuai et al., 2016) and the positive effects in reducing sugar degradation in acid solvolysis (Di Menno Di Bucchianico et al., 2023, 2022).

Although its valuable characteristics as a green and versatile solvent, the production of GVL never reached the industrial scale, and this is mainly due to the high production costs of the required reagents, such as LAs and ALs (Kerkel et al., 2021). The study of more cost-effective reaction paths, such as the production of ALs from biomass-derived monosaccharides like fructose, can promote the further development of GVL production from an industrial perspective. (Kerkel et al., 2021). The process design of GVL production from LCB-derived monosaccharides remains largely unexplored in the existing literature, leading to a lack of progression of this process to an industrial scale.

Although glucose is the most abundant hexose monomer in the lignocellulosic matrix, and therefore the most accessible and cost-effective substrate compared to other monomers (Peng et al., 2011), fructose has a higher molecular instability and faster reactivity in dehydration to the first intermediate towards ALs (An et al., 2017). The faster reaction kinetic results in high production yields (Démolis et al., 2014). Glucose, on the contrary, must undergo an initial isomerization step to fructose, resulting in slower conversion kinetics and lower production yields to ALs (Peng et al., 2011). Furthermore, from a catalyst perspective, the simultaneous action of isomerization and solvolysis requires the activity of more complex catalyst, with a dual acid nature (Zou et al., 2014).

Although some studies investigated the efficiency in terms of ALs yields of certain heterogeneous catalysts, few studies in the literature present kinetic modelling of glucose monomer conversion to ALs. On the contrary, the literature concerning fructose is more solid and in-depth, also describing the degradation to humins or the dissolution effect of fructose at high concentrations (Flannelly et al., 2015; Di Menno Di Bucchianico et al., 2023). Therefore, we focused on a GVL production process starting from fructose.

In this context, this article aims to explore, through a process design and techno-economic analysis, a process to produce GVL from LCB-derived fructose at industrial scale, via hydrogenation of BL as

intermediate. Delving into technological and economic aspects, this analysis aims to show feasibility, identify potential obstacles, and suggest improvements for the process.
As indicated by Cherubini et al. (Cherubini, 2010), the design of a sustainable biorefinery system cannot detached from the supply of a feedstock that is renewable, available and regular, and that is site-specific; therefore, this study is contextualized in a real-case study in the European context: the Normandy region in France that is well-known for the abundance and availability of second-generation LCB.
The site-specificity of the case study is considered within the techno-economic analysis by evaluating the effects of different production scales and energy supply systems in Normandy, where a process flow diagram of a potential GVL biorefinery from fructose is designed, from concept to process simulation, and optimization.
Based on economic key performance indicators (KPIs), the methodology applied in this work enables the identification of alternative configurations that show the highest potential profitability profile for the sustainable exploitation of waste LCB, constituting a preliminary outcome for a broader decision-making analysis of the investment in the initiative.

2. Material and Methods

The techno-economic analysis conducted in this paper is carried out with the following steps: (1) Definition of the conceptual design of process for the production of GVL from LCB-derived fructose; (2) Process modelling and optimization; (3) Evaluation of the alternatives for the energy supply to the production process; (4) Economic analysis of the alternative scenarios using KPIs; (5) Sensitivity and uncertainty analysis of the results obtained to check their robustness.

2.1 Conceptual process design

With the aim of developing the conceptual design for the production process of GVL from fructose, and on the basis of experimental and literature data (Delgado et al., 2022; Di Menno Di Bucchianico et al., 2023), two catalytic processes are assumed and combined in series. The pretreatment process of LCB and production of fructose is out of the scope of the present work, nevertheless, the associated economic impacts are considered within the economic analysis.
The production process of GVL from fructose is based on two main catalytic reactions, namely (i) the acid solvolysis of fructose to BL, and (ii) BL hydrogenation to GVL; the reactions, shown in Fig. 1(a), are carried out in two different process units in series.
In literature, the synthesis of GVL is carried out by hydrogenation of LA or ALs over a metal catalyst and through a two-step mechanism, where an intermediate is formed and cyclized; using gas hydrogen, the yield are recorded, avoiding the production of by-products (Dutta et al., 2019).
In particular, the synthesis of GVL from ALs has several advantages with respect to LA, such as a higher yield and the reduced metal leaching from the catalyst (Démolis et al., 2014). Several studies have analyzed the hydrogenation of ALs, highlighting the crucial effect of the reaction solvent in increasing productivity (Zhao et al., 2019). Among these, Capecci et al. (2021) investigated the use of GVL itself as solvent in the hydrogenation of BL, achieving yields of around 87% and eliminating the disadvantages of solvent separation steps. Based on this facts, in this work, we focused on GVL

production using hydrogenation of BL on Ru/C, and considering GVL as a solvent, as detailed by Delgado et al. (2022).

The design of a purification section between the solvolysis and the hydrogenation reactors is necessary, as well as a section to purify the final product to its market grade (i.e. >99%). A Block Flow Diagram of the process is reported in Fig. 1(b), and the details of each process block are explained in the following.

Based on literature reporting the size of similar existing plants (Conti Silva et al., 2022), a potential reference process size is 2 kt/y, thus corresponding to approximately 250 kg/h of GVL. Therefore, such productivity is assumed as a target to develop the conceptual design, and to perform the process simulation and optimization.

Concerning the first reaction stage, its conceptual design is based on the work of Di Menno Di Bucchianico et al. (Di Menno Di Bucchianico et al., 2023), where the reaction is catalyzed by an ion-exchange resin (Amberlite IR120) and in butanol-GVL solvent (ratio 70/30 wt%). The reaction is carried out at 20 bar and 110°C, feeding an initial fructose concentration of 100 g/L (stream 1 in Fig. 1 (b)), and obtaining an overall yield in BL of 78% for solid catalyst concentration of 130 g/L. Under these conditions, a complete conversion of fructose and the intermediates (i.e. 5-HMF and 5-butoxymethyl furfural, 5-BMF) is achieved, while other intermediates, i.e. LA and formic acid (FA) are not completely converted due to slower kinetics (Di Menno Di Bucchianico et al., 2023). Consequently, the outlet stream (i.e. stream 2 in Fig. 1 (b)) is made of BL, butyl formate (BF), water, LA, FA), GVL, butanol (BuOH), and degradation by-products (i.e. humins)(Di Menno Di Bucchianico et al., 2023).

Therefore, a separation step is designed to recover BL with LA (in traces) and GVL, to be sent to the hydrogenation reactor (stream 3). Humins, is also isolated in the separation unit, usually by means of filtration, since it is in an insoluble or partially soluble (Di Menno Di Bucchianico et al., 2023, 2021).

In the second reaction stage, the production of GVL through the hydrogenation of BL and LA in the presence of H_2-gas on a heterogeneous catalyst is design based on the work of Delgado et al. (Delgado et al., 2022), where the hydrogenation kinetic of BL over Ruthenium on activated carbon (Ru/C) and in GVL-solvent is studied. Under the reaction conditions reported in literature (i.e. 20 bar and 150 °C), the system reaches complete conversion of BL, considering a catalyst load of 1.7 g/L. The benefits of using GVL as solvent is also related to the improvement of downstream processes aimed at GVL recovery and purification (Delgado et al., 2022). Also in the present study, the use of GVL as solvent for both the reaction stages allows to simplify the downstream sections; in fact, the reaction products for hydrogenation (stream 5 in Fig. 1(b)) are sent to a single separation unit and to a purification unit, to isolate intermediate (i.e. butyl-4-hydroxyvalerate, BHP), then sent back to the hydrogenation reactor via stream 6, and separate the product of interest from the by-products (i.e. water and BuOH).

Finally, a purification of GVL from the reaction stream is needed: given the different boiling points (and high degradation temperatures), distillation is a suitable option for the separation. Once the required purity (>99 wt%) is reached, the GVL stream is split into the output final product stream (250 kg/h), and stream 10, in which GVL is partially recycled to the solvolysis reactor. Overall, we obtain a fructose-to-GVL yield of 50.5 wt%.

Secondary product, obtained from the separation stages are: BuOH, water, BF and FA in stream 7. Such stream is treated to remove water and FA first, and, the traces of BF from BuOH to be recirculated to the solvolysis reactor later.

In order to remove the aqueous phase (water and FA, that are miscible), from the BuOH-BF organic phase, it must be considered that BuOH, BF and water form a heterogeneous ternary azeotrope (Huiyuan and Songlin, 2006). A possible process solution is to carry out the separation by distillation, thus producing an anhydrous BuOH-BF mixture as bottom product, and a heterogeneous azeotrope mixture as head product; the latter mixture, can be sent to a liquid-liquid separator.
After water and FA removal, stream 8 is treated to separate BF from BuOH; the separation by distillation would require a train of distillation columns and and high energy demand, due to the low driving force of the process. For this reason, a catalytic reaction step of BF degradation is considered, where BF is decomposed to BuOH and CO by means of a metal oxide catalyst (e.g. Hydrotalcide/alumina-based catalyst) (Dai et al., 1998). As reported in the patent of Dai et al. (Dai et al., 1998), the reaction could be conducted in a fixed-bed reactor, at 120-260 °C and 6-40 bar, leading to a complete degradation. The regenerated BuOH (stream 9), is sent back to the solvolysis process, as illustrated in Fig. 1(b). A BuOH make-up stream is provided to make-up for losses and keep the solvent ratio constant.

2.2 Process modelling and optimization

Once the conceptual process scheme is defined, the process units are modelled and simulated on different scales, using the process simulator Aspen Hysys® V11 from Aspen Technology.
The simulation is carried out considering an initial production scale of 2 kt/y of GVL, with a purity >99.9% and overall fructose-to-GVL yield of 50.5 wt%; then further production scales are analyzed. The equation of state Benedict-Webb-Rubin-Lee-Startling is selected to estimate physicochemical and thermodynamic properties and phases equilibria, as it is particularly suitable for the simulation of the hydrogenation reactions (Leal Silva et al., 2018) and for chemical systems where BL, BuOH and GVL are present (Ariba et al., 2020). Furthermore, some properties (namely molecular weight, boiling temperatures, density, etc.) of fructose, BL, BHP and humins are taken from literature (Alamgir Ahmad et al., 2022; Kerkel et al., 2021).
The process flow diagram implemented in Hysys is shown in Fig. 2. In the construction of the preliminary process flow diagram, the sequential modular approach is used in the process modelling and simulation, linking several process units, auxiliary units, components, flows and selecting suitable thermodynamic methods. Once an initial reference process scheme is defined, the process scheme is evaluated at steady state, optimizing the process in terms of material recovery (i.e. recycling reactants and solvents to reaction units and purging unwanted compounds) and/or heat and energy recovery (i.e. high-temperature streams are used to heat and/or vaporize cold streams and vice versa). The material recovery, as for example the recycle of BuOH solvent (S42) and GVL (S23), is performed by using the logic unit, called '*recycle*', in the software. The recycle-block is a fictitious unit that allows the recycling of material streams, using an iterative guess-and-check algorithm, in order to converge, with a certain tolerance, the recycling loop.
In terms of energy recovery, streams with higher energy potential (e.g. hotter and/or cooler streams) are used to exchange heat with other process streams; as in E-100 in which stream S10 at high temperature is used to preconditioned the inlet stream S2 to the solvolysis reactor; or in E-103 heat exchanger where the S18 stream is used to partially heat S31 before the BF degradation unit, reducing the thermal power load required from the utility.

2.2.1 Solvolysis Fructose to n-butyl levulinate

The feeding stream to this section (stream S1 of Fig. 2) is made of fructose and solvent (BuOH-GVL) at ambient conditions (see Table 1). The stream is sent to a pump (P-100) and a heat exchanger (E-100) to be conditioned to the reaction conditions (20 bar and 110°C, stream S3 in Fig. 2). The solvolysis reactor is a Continuous stirred-tank reactor (CSTR) that is simulated in Aspen Hysys using an item called "*conversion reactor"* (CRV-100), with an overall BL yield of 78 mol%, considering the full conversion of fructose, and intermediates (5-HMF and 5-BMF), obtaining a product stream (S4, Fig. 2) made of BL and B, residual intermediates (e.g. LA, FA), by-products and solvents. The degradation by-products, humins, are present also in the stream with a maximum yield of 10 mol%. To simulate the separation of humins by filtration from the main products, the "*splitter*" (Sp-01) operator is used, assuming a complete separation.
Before purification via distillation, the stream obtained (S5, Fig. 2) is sent to a 2-phase separator (V-100), where it is depressurized to 2 bar to promote the removal of the dissolved CO resulting from the recirculation of BuOH from the BF decomposition unit. The light stream (S7 in Fig. 2) is sent to flaring. The heavy stream (S6 in Fig. 2, ~12 wt% in BL), is sent to an 8-stage distillation column (T-100), from which a bottom stream rich in GVL is obtained (S8 in Fig. 2, ~ 77 wt% of GVL, 22 wt% of BL and >1 wt% of LA), and is conveyed to the hydrogenation section. The light stream from the distillation column (S9 in Fig. 2), mainly composed of BuOH, BF, water and FA, is was, therefore, sent to the H_2O-FA separation unit.

2.2.2 Hydrogenation of n-butyl levulinate to γ-valerolactone

The outlet stream from the solvolysis (S8, Fig. 2) is mixed with a recycling stream rich in BHP (S21, Fig. 2) performing heat recovery (E-100) to the inlet conditions (S13, Fig. 2Fig. 2) of the hydrogenation reactor (CRV-101, working at 150 °C and 20 bar), once again using a pump (P-101) and a heat exchanger (E-101). Also in this case, the reactor is a CSTR that is simulated in Aspen Hysys using a conversion reactor. A stream of H_2-gas (S14, Fig. 2) is fed to the reactor (prior heating, using E-102) with a molar flow rate that ensures complete stoichiometric conversion to the hydrogenation intermediates (i.e. BHP and HPA). Given the kinetics of the cyclization reaction (Delgado et al., 2022), the conversion of BHP to GVL is not complete (~ 80%); thus, the output stream (S16, Fig. 2) from the reactor had ~ 8 wt% of BHP and ~ 77 wt% of GVL, together with BuOH and H_2O as secondary products. Therefore, a train of two distillation columns is designed. The first column (T-101, 11 stages) is designed to separate BuOH and H_2O (S17, Fig. 2) from GVL and BHP (S18, Fig. 2). S18 (~ 92 wt% GVL) is sent (prior heat recovery in E-103) to the second distillation column (T-102, 13 stages), to achieve the required marked purity specifications for GVL (S20, > 99.9 wt%); the bottom stream (S21, > 38.3 wt% in BHP) is s recycled to the hydrogenation reactor.
Finally, the stream of GVL (S20, Fig. 2Fig. 2) is cooled down (in E-108), giving the final product stream (S22 in Fig. 2Fig. 2), and partially recycled to the solvolysis block (S23 in Fig. 2Fig. 2).

2.2.3 Water-formic acid separation and butyl formate decomposition

The streams resulting from the purification units (S9 from T-100 and S17 from T-101) are mixed and conveyed to the water separation unit; the resulting stream (S24 in Fig. 2, BuOH ~ 84 wt%, BF~ 10 wt%, and H_2O ~ 6 wt%) is sent to the last a distillation column (T-103, 12 stages).

BuOH, BF and H_2O form a minimum-boiling heterogeneous ternary azeotrope, thus separation is carried out by considering a distillation, where anhydrous BuOH-BF mixture (> 10 %wt in BF) is obtained as bottom product (S30 of Fig. 2Fig. 2), whereas the ternary azeotropic mixture (S25 of Fig. 2), is the top vapor product stream. After condensation (E-104), the S26 is sent to a decanter (V-101) in which aqueous vs. organic phase (S27, S29, Fig. 2), are separated. While the aqueous phase (S27, > 93 wt% in H_2O) is sent to wastewater treatment, the organic phase (S29) is fed back to T-102 to increase the recovery rate from the bottom.
As the mixture of BuOH-BF (S30 of Fig. 2) would be a highly-energy intensive distillation (Dai et al., 1998), due to the reduced driving force, a different strategy is designed and implemented: the stream is preconditioned (S33, Fig. 2Fig. 2) and fed to a catalytic reactor (CRV-102), where BF is fully converted to CO and BuOH by means of heterogeneous catalysis (metal oxides catalyst DHT-4A/Alumina, at 190 °C and 20 bar, (Dai et al., 1998)). CRV-102 is simulated as a conversion reactor, whose product stream at gas state (S34, Fig. 2) is partially condensed to recover part of the BuOH entrained in the gas, and conveyed into the liquid product stream (S35, Fig. 2Fig. 2) via a gas-liquid separator (V-102). Stream S39 (BuOH > 99.5 wt%) is cooled down (in E-107), sent to a separator (V-103) to remove the residual CO content released in the cooling and finally recycled (S42, Fig. 2) as a solvent to the solvolysis block. The CO streams from the separators (S37, and S41) are conveyed to S7 and sent to flare. A fresh BuOH stream is considered in order to adjust the concentration specs at the reactor feed.

2.2.4 Thermal utility systems

In parallel with the design of the process scheme, the thermal utility systems are designed. Based on the thermal requirements of the different process units and operating temperatures, as shown in Table 2, the main thermal fluids considered are: high-pressure steam, chilling water, cooling water.
Table 2 shows the two reaction units (CRV-100 and CRV-101) with the highest heat flux to be absorbed, followed by the column bottom reboilers (Reb-102, Reb-103) and the reactor (CRV-102) that require a high-temperature utility instead.
For the high-temperature utility, a high-pressure steam generation cycle (45 bar, 250°C) is used, simulating steam production and heat exchange with the process fluids by reproducing the main process heat exchangers (E-101, R-100, etc.), allocating the service fluid on the shell/pipe side. On the basis of the heat demand of the process, the steam flow rate in the cycle and the heat demand in the boiler are evaluated; depending on the type of boiler (natural gas, biomass or electric) different energy scenarios are presented in the next subsection.
The cooling water is supplied to the system at 30°C and returns to the cooling tower at 40°C. The cooling water circuit is designed considering the required cooling power output and also simulating the required airflow to cool the water. After sizing the circuit in terms of airflow, the electrical demand associated with the cooling tower is based on literature data from data sheets of commercially available technologies (W-tech, 2022). Instead, chilled water is supplied at 5°C through a propane refrigeration circuit (Anand et al., 2013). The typical one-stage propane refrigeration cycle is designed and sized on the basis of the required propane flow rate and considering the electrical energy demand on the cycle's compressor (Anand et al., 2013).

2.3 Evaluation of alternatives for the energy supply to the production process

Different configurations for the energy supply to the process are identified on the basis of the required thermal power, through the production of high-pressure steam as thermal utility. In this study, three alternative configurations are considered: (i) natural gas-fueled boiler; (ii) biomass-fueled boiler; and (iii) electric boiler.

The conventional natural gas system has an efficiency of 87.7 %, while it was set at 89.9 % for a biomass-fueled system (Villeneuve et al., 2012). In this case the required heat output could be provided by using LCB, considering for it an average higher heating value (HHV) of 19 MJ/kg (Esteves et al., 2023). The reaction by-product humins is included as a combustible source for this configuration, together with LCB, since it has a heating value estimated in the literature around 19.5 MJ/kg (Muralidhara et al., 2018). In contrast to these two scenarios, a fully electrified scenario is included in the investigation. The latter scenario was implemented to mimic a decarbonization strategy, where electrification and the use of low-carbon electricity is a meant to reduce emissions; the electric boiler was considered to have an efficiency of 100% based on literature specifications (Van Wortswinkel and Nijs, 2010).

Having defined the different energy configurations, the analysis also includes the scale effect, analyzing different production sizes in accordance with the availability of biomass at the investigated site.

Normandy region has an annual waste LCB production of over 400 kt/y (per capita value of 133.6 kg, compared to 79.3 kg nationally), of which only 46% is currently valorized (Biomasse Normandie et al., 2020). Based on current sugar monomer production technologies in the literature and their average yields: 18-37.8% for glucose, and about 11-15% for fructose (Kwan et al., 2019; Marianou et al., 2016), the availability of LCB in the region can provide over 30 kt/y of fructose to sustain the productivity of the potential GVL biorefinery.

Given the availability of LCB and the overall yield of the proposed fructose-to-GVL process, the potential production of GVL is between 10-22 kt/y. For this reason, the scale effect of the plant is analyzed by considering sizes of 2, 4 kt/y and, conservatively, 10 kt/y.

Therefore, the study identifies and analyzes 9 different scenarios:

- Scenario 1 (SC#1): production size of 2 kt/y and fueled by natural gas.
- Scenario 2 (SC#2): production size of 2 kt/y and fueled by biomass.
- Scenario 3 (SC#3): production size of 2 kt/y and fueled by electricity.
- Scenario 4 (SC#4): production size of 4 kt/y and fueled by natural gas.
- Scenario 5 (SC#5): production size of 4 kt/y and fueled by biomass.
- Scenario 6 (SC#6): production size of 4 kt/y and fueled by electricity.
- Scenario 7 (SC#7): production size of 10 kt/y and fueled by natural gas.
- Scenario 8 (SC#8): production size of 10 kt/y and fueled by biomass.
- Scenario 9 (SC#9): production size of 10 kt/y and fueled by electricity.

2.4 Economic analysis

The economic analysis of the scenarios was based on the following key performance indicators (KPIs):

1. Net Present Value (NPV)

2. Internal Rate of Return (IRR)
3. Minimum Selling Price (MSP)
4. Levelized Cost of Product (LCOP)

The NPV indicator enables to define the profit value generated by an initiative over its lifetime and it is expressed as follows in *Eq.1* (Casson Moreno et al., 2020):

$$NPV[€] = \sum_{n}^{N} \frac{F_n}{(1+r)^n} - I = \sum_{n}^{N} \frac{[R_n - OPEX - D] \cdot (1 - Tax) + D}{(1+r)^n} - I \qquad Eq.1$$

where F_n is the cash flow (€/y) generated in n-th year, discounted with the rate *r*, while *I* (€) is the initial capital investment (i.e. CAPEX). F_n is calculated on the basis of the net profit before taxation, given by the revenues (R_n) reduced by annual operating expenses (OPEX) and depreciation (*D*) that, multiplied by the taxation rate $(1 - Tax)$, generates the net profit after taxation in the n-th year, and to which *D* is added back. *D* is evaluated by the straight-line method and annually fixed to the 4% of the fixed capital investment (Towler and Sinnott, 2008). The discount rate is assumed to be 8 %, as average value for biomass-application processes and new energy installations (Casson Moreno et al., 2020). The NPV allows also to calculate the pay-back period of the investment, which is the year at which NPV reaches zero; from that moment on, the production process will result in a net profit.

The Internal Rate of Return (IRR) is evaluated to determine the attractiveness of the investment; the IRR is the value of the discount rate corresponding to a cumulative NPV-zero at the end of the plant's life (N-year), therefore it represents the highest *r* that justifies the investment. The index is defined as follows in *Eq.2* (Casson Moreno et al., 2020):

$$r = IRR\ for\ which\ NPV = 0 \qquad Eq.2$$

In general, the higher the IRR, the more desirable the investment to be undertaken, and when comparing investment options with other similar characteristics, the investment with the highest IRR is likely to be considered the best (Casson Moreno et al., 2020).

MSP is also calculated, that is the price of the product that determines a zero NPV for a given discount rate at the end of the plant's life (or at a specified year of interest), and thus represents the minimum selling price for a favorable initiative; the index is defined according to the following Eq.3 (Chen et al., 2011):

$$MSP\left[\frac{€}{kg}\right] for\ which\ NPV = 0 \qquad Eq.3$$

A lower MSP index value denotes an initiative with higher income flexibility and lower production costs.

Lastly, the Levelized Cost Of Product represents the averaged production cost of the product per unit over the lifetime of the production scheme and it is defined as follows in Eq.4 (Casson Moreno et al., 2020):

$$LCOP\ \left[\frac{€}{kg}\right] = \frac{CAPEX + \sum_{n}^{N} \frac{OPEX}{(1+r)^n}}{\sum_{n}^{N} \frac{P_i}{(1+r)^n}} \qquad Eq.4$$

where CAPEX are the capital expenditures, and P_i is the annual production of the product i-th (kg/y). Being a cost index, the initiative is cost-effective for low index values, which therefore correspond to lower unit production costs.

2.4.1 Economic assumptions

The main economic parameters, and assumptions used in this study are shown in Table 3. The fixed capital investment (FCI) is, generally, defined by the sum of internal battery boundary costs (ISBL), such as purchase and installation of equipment, instrumentation, controls, piping and electrical systems; external battery boundary costs (OSBL), such as costs of buildings and utility facilities, indirect costs, contingency costs. Some methods evaluate the different cost items of ISBL and OSBL by means of indices proportional to the cost of the installed equipment (Towler and Sinnott, 2008). In this work, the FCI is evaluated using the Aspen Process Economic Analyzer; based on the process parameters (temperature, pressure, mass flow rate and duty), the software was used to size and estimate the purchased cost of the main process equipment (heat exchangers, columns, reactors, pumps, process vessels, etc.). The software also evaluates FCI on the basis of installation costs which are updated with data collected from engineering, procurement, and construction companies and equipment manufacturers (Haydary, 2018). For utility-equipment (cooling water tower, steam-generation boiler, etc.), the sizing and cost-evaluation is based on commercial datasheets and literature data (Abdin et al., 2021; W-tech, 2022). The costs obtained for each equipment item at each production size evaluated are reported in Table 4.
Then, the total capital investment (CAPEX) is calculated as the sum of fixed capital, working capital and start-up capital, which are defined in Table 3. The plant's lifetime is set to 25 years (8400 h/y), assuming the FCI is invested over a construction period of 2 years, with 20% and 80% in the first (year 1) and second (year 0) respectively. Depreciation is calculated using a straight-line method among a period of 25 years. A discounted cash flow analysis is performed to estimate the minimum product selling prices (MSP), net present value (NPV), and cost of production.
The annual operating cost (OPEX) is defined as the sum of variable operating expenses (VOE), fixed operating expenses (FOE) and general operating expenses (GOE); the variable annual portion of expenses accounts for the costs of raw materials, utilities (heating and cooling systems), catalysts, make-up, wastewater treatment and waste disposal. The fixed expenses take into account the annual cost of operational labor, estimated by considering 3 operators per shift, one for each process section (solvolysis section; hydrogenation section; solvent regeneration section), 5 shifts, and with a salary of €32 per hour, referring to the cost of labor in France in 2022 (EUROSTAT, 2022).
All equipment and material costs are updated to 2022-€ prices, considering the 2022-CEPCI index (Chemical Engineering Plant Cost Index), average currency conversion value USD/€-2022, and location factor 1.13, referred to France (Towler and Sinnott, 2008).
In the evaluation of raw material costs, the cost of the fructose supply is considered by reporting the literature cost for fructose derived from waste biomass; $747/ton is assumed from the work of Kwan et al. (Kwan et al., 2019) on the production of a high-fructose syrup from waste biomass. This cost item is, however, indirectly discounted by the avoided disposal cost of the biomass required to produce fructose, which averages 76.5 €/ton (considering disposal by incineration and landfilling) (UpCycle, 2019). The avoided disposal cost is reported with a negative sign in the waste disposal cost item. For hydrogen and GVL, an updated market range to 2022 is reported. For GVL, the most up-to-date price range in the literature considers a price between 1.18 and 3.65 €/kg referred to 2019

(Byun and Han, 2019); by adjusting the price limits through CEPCI-2022, with an increase to 1.6 - 4.9 €/kg. For hydrogen, the production cost is 1.4-1.8 €/kg from steam reforming, as reported in 2020 (Hydrogen Council, 2020). The increase in the cost of natural gas in 2021-2022 led to a surge in the production cost of hydrogen to 4.8 €/kg at the end of 2021 (Hydrogen Council, 2020). Considering the costs of hydrogen transport and distribution, the final cost increases further by 50-60%. For these reasons, the cost of hydrogen in this analysis is in the range of 4.8-7.65 €/kg, as shown in Table 5.

2.5 Sensitivity and uncertainty analysis

Given the uncertainties of some inputs parameters to the economic analysis, a sensitivity and uncertainty analysis are performed to evaluate the robustness of the results obtained for each scenario, and the impact of the parameters, such as annual operating costs, fixed capital investment, GVL selling price, discount rate, tax rate and price of raw materials and catalysts, on the profitability of the initiative (Okolie et al., 2021).

The analysis was conducted using the Monte Carlo method, which is widely used in many fields of science to determine the variability of results, given an uncertainty on the inputs.

In this work, we varied the main economic parameters in a range of ±20 % with respect to the values reported in Table 3, according to a uniform distribution, and considering a sample of 10^5 possible combinations for the results (Cipolletta et al., 2022) to quantify and assess the economic risk associated with the project.

3. Results and Discussion

3.1 Energy analysis

In this section, the results of the energy analysis for the process carried out at different production scales and evaluating different scenarios for the energy supply are discussed.

The energy analysis of the baseline process scheme (2 kt/y of GVL) is conducted, obtaining an electrical power demand of 0.78 MW, which is mainly determined by the consumption at the compressor of the cooling cycle, the evaporative tower for cooling water, and a thermal power demand by the steam boiler (1.92 MW). Then, the thermal power demand is reduced by 7.5% through the integration of heat recovery between process streams.

The same analysis is extended to larger plant sizes, such as 4 kt/y and 10 kt/y, obtaining the results shown in Table 5.

After energy integration with heat exchanger network design, the process's heating requirements decreased by between 7-8.7%, in both production sizes. As shown in Table 5, electrical and thermal power requirements are directly proportional to plant productivity, being twofold for 4 kt/y productivity and slightly less than fivefold (ca. 4.8-4.9) for the 10 kt/y size, compared to the 2 kt/y size. This effect of scale is also proportionally reflected in the flow rate of utilities to be supplied in the different energy scenarios.

Based on the energy demands, the different scenarios presented are analyzed. Besides the use of natural gas and electricity, in terms of LCB, the thermal power demand can be covered by 405 kg/h for the production size of 2 kt/y (SC#2); the amount of biomass for bio-energy production can be further reduced by more than 12% (355 kg/h) considering humins as an energy source. Humins is also integrated into the biomass demand at 4 kt/y (728 kg/h (SC#5)), and at 10 kt/y (1718 kg/h (SC#8).

The bioenergy-based scenario also allows for full utilization of a reaction byproduct, reducing LCB demand and directly affecting the economic profile of the initiative.

3.2 Economic analysis

In this section, we discuss the results of the economic analysis for the process at different production scales (i.e. 2, 4, and 10 kt/y), considering the different scenarios for the energy supply defined in section 2.3.

Even if the contribution of the FCI to the CAPEX decreases when increasing the production capacity of the plant (from 88% to 82%, see Table 6), designing a larger scale causes and increase in the overall economic investment of +17% and further +75% when moving from 2 kt/y to 10 kt/y. More in details, accounting working capital and start-up capital together with fixed capital, as shown in Table 6, the total initial investment is estimated in the range of 19.2-19.5 M€ for the production size of 2 kt/y, depending on the different energy source scenario for heat demand; for higher production capacities, the investment increases up to 22.6-23.4 M€ for 4 kt/y of GVL production and up to 34.6-36.3 M€ for 10 kt/y.

In terms of annual operating expenses, variable operating expenses present the major impact on the operating cost of the initiative, due to the high contribution of raw material and utility costs, as listed in Table 6Table 6. For the analyzed plant sizes, the full electric configurations (i.e. SC#3, SC#6, SC#9) have higher operating costs due to the cost of electricity from the national grid. In contrast, in the scenarios in which thermal power is derived from biomass (i.e. SC#2, SC#5, SC#8), utility supply costs are lower, thanks also to the use of humins generated by the process as a heating source.

The analysis of the economic KPIs indicates that the biomass-fueled scenario is the only economically viable scenario for the smallest production size in terms of NPV and a return on initial investment in 15 years considering, when an average market price of 3.26 €/kg. The discounted PBP and NPV generated by the end-of-life initiative (NPV25) are evaluated considering the income generated with the average market sale price.

The comparison of the IRR shows that the only economically favorable scenario at 2kt/y production scale is the biomass-fueled one (SC#2)~~;~~ as only this scenario has an IRR higher than the current discount rate used in the analysis (11% vs 8%).

By increasing the production scale to 4 kt/y, the natural gas-fired scenario (SC#4) manages to pay back the initial investment after 10 years, with a competitive MSP compared to the current market price (i.e. 2.8 vs 3.26 €/kg) and a favorable IRR of 15%. The scale effect also increases the profitability of the biomass scenario (SC#5), which remains the most profitable scenario for this size as well, with a reduced PBP compared to its smaller size counterpart, reduced MSP, and higher IRR. The electricity-fueled scenario (SC#6) continues to be unprofitable, i.e. unfavorable economic KPIs, for the 4 kt/y size, reaching potential profitability only for the largest production size. The results related to MSP of the different scenarios are depicted in Fig. 4(a).

In fact, the SC#9 scenario achieves potential profitability at the higher production scale (10 kt/y of GVL), where the PBP is the lowest recorded (8 years), a 32.7 M€ NPV, MSP below the average market price, and an IRR above 8%; however, the achieved NPV is lower than that generated by the NG-fueled scenario (SC#7), which is about twice as high, and by the LCB-based scenario (SC#8), which is more than 3.5 times higher, resulting also for this size the most profitable energy scenario.

The LCB-fueled scenario therefore has the highest economic profile in all production classes (Fig. 3 (a)), with the highest IRR index, meaning that the investment to be undertaken is the most desirable.

This result can be attributed to the trend in operating costs and hence the production cost index (LCOP) being the lower in each production size for the LCB-scenario, where the lowest is obtained at 10 kt/y (SC#8), where the GVL production cost results 1.89 €/kg, - 42% with respect to the 2 kt/y size (SC#2), and - 20% and - 36% with respect to the NG- (SC#7) and electricity-fueled (SC#9) scenarios for the same production capacity. The results related to LCOP of the different scenarios are visible in Fig. 4(b).
As also shown in Fig. 3(b)(c)(d), the increase in the scale of production from 2 to 10 kt/y leads to an increase in the profitability of the initiative, with a reduction of the PBP and an increase in the cumulative cash flow at the end of life, with the same energy-scenario. Furthermore, for the same size of 10 kt/y and thus for the same initial investment in year zero, the biomass-fueled scenario shows a significantly sharper growth trend of the NPV index and thus higher end-of-life profitability.

3.4 3 Results of the sensitivity and uncertainty analysis

The sensitivity and uncertainty analysis is carried out considering the variation of the main economic parameters reported in Fig. 5. In Fig. 5(a), the cumulative probability of the NPV index for all scenarios and capacities is shown. Over all iterations, combinations of scenarios with respect to the NPV index are evaluated and ranked, identifying the scenario with the highest profitability. Based on the iterations, the scenario with the lowest probability of loss (probability of NPV being lower or equal to 0) is SC#9, with a probability of 22%, and a mean NPV of around 60 M€, as seen from the NPV distribution shown in Fig. 5(a). In Fig. 5(b), the overall probability of occurrence of each scenario to be the best in terms of NPV value, is shown. From the comparison, it can be seen that the biomass-fueled scenarios are the only ones with non-zero probability of occurrence as first scenario; in particular, SC#9 scenario is the one with the highest probability (91%) of occurrence as the most profitable scenario, with the highest value of NPV.
Overall, therefore, the biomass-fueled energy scenario presents the highest profitability for all plant sizes and with high revenue for a capacity of 10 kt/y (SC#8).
In addition to overall, the 10 kt/y plant size is also most likely to be the most profitable configuration by energy category, as indicated by Fig. 5(b)(c)(d) for the natural gas, biomass, and electricity scenarios. Compared to the intermediate size of 4 kt/y (SC#4, SC#5, SC#6), the smaller size of 2 kt/y (SC#1, SC#2, SC#3) has a higher probability of occurrence as first scenario, but this can be attributed to overall negative NPV for the different sizes, thus less negative for the smaller size.
A sensitivity and uncertainty analysis are also conducted to identify the parameters that have the greatest impact on NPV, as shown in Fig. 6. It can be observed that the selling price of GVL, annual operating costs of feedstock and catalyst have the greatest impact on the NPVs for all the energy supply scenarios. For example, with a 5% increase in the sales price of GVL, NPV increased by 55.6%, 50.4%, and 20.2%, in NG (Fig. 5(a)), Biomass (Fig. 6(b)), and Electricity scenarios respectively (Fig. 6(c)); more moderate are the variation effects in the fully electrified scenario. For this scenario, NPV is more sensitive to the variation of the electricity price, which varies by ±10.3%, compared to ±9% in the NG-Scenario and ±8.2% in the Biomass-Scenario. On the other hand, the NG scenario has a 13% reduction in NPV, as a result of the 5% increase in the NG price. Overall, the hydrogen cost, taxation index and discount rate have an effect of less than 5% variation in the profitability of the scenarios.

4. Conclusions

A novel GVL production process from biomass-derived fructose is developed, integrating an acid solvolysis unit with a hydrogenation unit. Rigorous simulation models are employed for process and service units, and energy integration minimized utility requirements. Considering a case study in Normandy, the economic analysis of the process focused on scale effect and energy scenarios. Results highlights the biomass-fueled scenarios as most profitable across all production scales, with the 10 kt/y scale exhibiting the lowest minimum selling price for GVL (i.e. 1.89 €/kg) and highest end-of-life revenue (i.e. 113 M€). Biomass emerged as a cost-effective bioenergy source, supporting industrial-scale GVL production profitability.

References

1. Abdin, Z., Tang, C., Liu, Y., Catchpole, K., 2021. Large-scale stationary hydrogen storage via liquid organic hydrogen carriers. iScience 24, 102966. https://doi.org/10.1016/j.isci.2021.102966
2. Alamgir Ahmad, K., Haider Siddiqui, M., Pant, K.K., Nigam, K.D.P., Shetti, N.P., Aminabhavi, T.M., Ahmad, E., 2022. A critical review on suitability and catalytic production of butyl levulinate as a blending molecule for green diesel. Chemical Engineering Journal 447, 137550. https://doi.org/10.1016/j.cej.2022.137550
3. An R, Xu G, Chang C, Bai J, Fang S. Efficient one-pot synthesis of n-butyl levulinate from carbohydrates catalyzed by Fe 2 (SO 4) 3. Journal of Energy Chemistry 2017;26:556–63. https://doi.org/10.1016/j.jechem.2016.11.015.
4. Anand, S., Gupta, A., Tyagi, S.K., 2013. Simulation studies of refrigeration cycles: A review. Renewable and Sustainable Energy Reviews 17, 260–277. https://doi.org/10.1016/j.rser.2012.09.021
5. Ariba, H., Wang, Y., Devouge-Boyer, C., Stateva, R.P., Leveneur, S., 2020. Physicochemical Properties for the Reaction Systems: Levulinic Acid, Its Esters, and γ-Valerolactone. J. Chem. Eng. Data 65, 3008–3020. https://doi.org/10.1021/acs.jced.9b00965
6. Ashokkumar, V., Venkatkarthick, R., Jayashree, S., Chuetor, S., Dharmaraj, S., Kumar, G., Chen, W.-H., Ngamcharussrivichai, C., 2022. Recent advances in lignocellulosic biomass for biofuels and value-added bioproducts - A critical review. Bioresource Technology 344, 126195. https://doi.org/10.1016/j.biortech.2021.126195
7. Baddour, F.G., Snowden-Swan, L., Super, J.D., Van Allsburg, K.M., 2018. Estimating Precommercial Heterogeneous Catalyst Price: A Simple Step-Based Method. Org. Process Res. Dev. 22, 1599–1605. https://doi.org/10.1021/acs.oprd.8b00245
8. Baral, N.R., Shah, A., 2016. Techno-Economic Analysis of Cellulosic Butanol Production from Corn Stover through Acetone–Butanol–Ethanol Fermentation. Energy Fuels 30, 5779–5790. https://doi.org/10.1021/acs.energyfuels.6b00819
9. Biomasse Normandie, Région Normandie, ADEME, 2020. Observatoire des déchets de Normandie - Les déchets ménagers et assimilés en Normandie - Année 2018. Observatoire des déchets de Normandie.
10. Byun, J., Han, J., 2019. Catalytic conversion of corn stover for 〈gamma〉-valerolactone production by two different solvent strategies: Techno-economic assessment. Energy 175, 546–553. https://doi.org/10.1016/j.energy.2019.03.070
11. Capecci S, Wang Y, Casson Moreno V, Held C, Leveneur S. Solvent effect on the kinetics of the hydrogenation of n-butyl levulinate to γ-valerolactone. Chemical Engineering Science 2021;231:116315. https://doi.org/10.1016/j.ces.2020.116315
12. Casson Moreno, V., Iervolino, G., Tugnoli, A., Cozzani, V., 2020. Techno-economic and environmental sustainability of biomass waste conversion based on thermocatalytic reforming. Waste Management 101, 106–115. https://doi.org/10.1016/j.wasman.2019.10.002
13. Chen, H., Yu, B., Jin, S., 2011. Production of levulinic acid from steam exploded rice straw via solid superacid, S2O82-/ZrO2–SiO2–Sm2O3. Bioresource Technology 102, 3568–3570. https://doi.org/10.1016/j.biortech.2010.10.018

14. Cherubini, F., 2010. The biorefinery concept: Using biomass instead of oil for producing energy and chemicals. Energy Conversion and Management 51, 1412–1421. https://doi.org/10.1016/j.enconman.2010.01.015
15. Christensen, E., Williams, A., Paul, S., Burton, S., McCormick, R.L., 2011. Properties and Performance of Levulinate Esters as Diesel Blend Components. Energy Fuels 25, 5422–5428. https://doi.org/10.1021/ef201229j
16. Cipolletta, M., D'Ambrosio, M., Casson Moreno, V., Cozzani, V., 2022. Enhancing the sustainability of biodiesel fuels by inherently safer production processes. Journal of Cleaner Production 344, 131075. https://doi.org/10.1016/j.jclepro.2022.131075
17. Conti Silva, J.A., Grilo, L.M., Vasconcelos, M.H., Lacerda, T.M., 2022. Levulinic acid: perspectives of its biobased production and most promising derivatives, in: Production of Top 12 Biochemicals Selected by USDOE from Renewable Resources. Elsevier, pp. 387–414. https://doi.org/10.1016/B978-0-12-823531-7.00002-0
18. Dai, P.-S.E., Neff, L.D., Preston, K.L., Hwan, R.-Y.J., 1998. CATALYTIC DECOMPOSITION OF FORMATE IMPURITES INTERTARY BUTYLALCOHOL AND METHYL TERTARY BUTYL ETHER STREAMS. Patent Number: 5,723,698.
19. Delgado, J., Vasquez Salcedo, W.N., Bronzetti, G., Casson Moreno, V., Mignot, M., Legros, J., Held, C., Grénman, H., Leveneur, S., 2022. Kinetic model assessment for the synthesis of γ-valerolactone from n-butyl levulinate and levulinic acid hydrogenation over the synergy effect of dual catalysts Ru/C and Amberlite IR-120. Chemical Engineering Journal 430, 133053. https://doi.org/10.1016/j.cej.2021.133053
20. Démolis A, Essayem N, Rataboul F. Synthesis and Applications of Alkyl Levulinates. ACS Sustainable Chem Eng 2014;2:1338–52. https://doi.org/10.1021/sc500082n.
21. Di Menno Di Bucchianico, D., Buvat, J.-C., Mignot, M., Casson Moreno, V., Leveneur, S., 2022. Role of solvent in enhancing the production of butyl levulinate from fructose. Fuel 318, 123703. https://doi.org/10.1016/j.fuel.2022.123703
22. Di Menno Di Bucchianico, D., Mignot, M., Buvat, J.-C., Casson Moreno, V., Leveneur, S., 2023. Production of butyl levulinate from the solvolysis of high-gravity fructose over heterogeneous catalyst: In-depth kinetic modeling. Chemical Engineering Journal 465, 142914. https://doi.org/10.1016/j.cej.2023.142914
23. Di Menno Di Bucchianico, D., Wang, Y., Buvat, J.-C., Pan, Y., Casson Moreno, V.C., Leveneur, S., 2021. Production of levulinic acid and alkyl levulinates: A process insight. Green Chem. https://doi.org/10.1039/D1GC02457D
24. Ding, S., Zhang, H., Li, B., Xu, W., Chen, Xuefang, Yao, S., Xiong, L., Guo, H., Chen, Xinde, 2022. Selective hydrogenation of butyl levulinate to γ-valerolactone over sulfonated activated carbon-supported SnRuB bifunctional catalysts. New J. Chem. 46, 1381–1391. https://doi.org/10.1039/D1NJ04800G
25. Dutta S, Yu IKM, Tsang DCW, Ng YH, Ok YS, Sherwood J, et al. Green synthesis of gamma-valerolactone (GVL) through hydrogenation of biomass-derived levulinic acid using non-noble metal catalysts: A critical review. Chemical Engineering Journal 2019;372:992–1006. https://doi.org/10.1016/j.cej.2019.04.199
26. Dutta, S., Yu, I.K.M., Tsang, D.C.W., Su, Z., Hu, C., Wu, K.C.W., Yip, A.C.K., Ok, Y.S., Poon, C.S., 2020. Influence of green solvent on levulinic acid production from lignocellulosic paper waste. Bioresource Technology 298, 122544. https://doi.org/10.1016/j.biortech.2019.122544
27. EI, 2023. Statistical Review of World Energy 2023.
28. Esteves, B., Sen, U., Pereira, H., 2023. Influence of Chemical Composition on Heating Value of Biomass: A Review and Bibliometric Analysis. Energies 16, 4226. https://doi.org/10.3390/en16104226
29. EUROSTAT, 2022.
30. Fernández Méndez, J., Farfan Orozco, F., Ladero Galán, M., Grénman, H., 2023. Techno-economic evaluation of obtaining valuable rare sugars from thermo-mechanical pulping side streams utilizing the latest technology. Chemical Engineering Journal 455, 140852. https://doi.org/10.1016/j.cej.2022.140852
31. Flannelly T, Dooley S, Leahy JJ. Reaction Pathway Analysis of Ethyl Levulinate and 5-Ethoxymethylfurfural from D-Fructose Acid Hydrolysis in Ethanol. Energy Fuels 2015;29:7554–65. https://doi.org/10.1021/acs.energyfuels.5b01481
32. Haydary, J., 2018. Chemical Process Design and Simulation: Aspen Plus and Aspen Hysys Applications. John Wiley & Sons, Inc., Hoboken, NJ, USA. https://doi.org/10.1002/9781119311478

33. Huiyuan, W., Songlin, X., 2006. Separation of *tert* -Butyl Alcohol-Water Mixtures by a Heterogeneous Azeotropic Batch Distillation Process. Chem Eng & Technol 29, 113–118. https://doi.org/10.1002/ceat.200500245
34. Hydrogen Council, 2020. Path to hydrogen competitiveness A cost perspective. Hydrogen Council.
35. IEA, 2021. Net Zero by 2050. IEA, Paris.
36. Kang, C., Liu, J.J., Woo, N., Won, W., 2023. Process Design for the Sustainable Production of Butyric Acid Using Techno-Economic Analysis and Life Cycle Assessment. ACS Sustainable Chem. Eng. 11, 4430–4440. https://doi.org/10.1021/acssuschemeng.2c07372
37. Kerkel, F., Markiewicz, M., Stolte, S., Müller, E., Kunz, W., 2021. The green platform molecule gamma-valerolactone – ecotoxicity, biodegradability, solvent properties, and potential applications. Green Chem. 23, 2962–2976. https://doi.org/10.1039/D0GC04353B
38. Kisuma Chemicals, 2023. Kisuma Chemicals – DHT-4A [WWW Document]. Kisuma Chemicals – Continuity through Innovation. URL https://webshop.kisuma.com/dht-4a.html
39. Kwan, T.H., Ong, K.L., Haque, M.A., Kulkarni, S., Lin, C.S.K., 2019. Biorefinery of food and beverage waste valorisation for sugar syrups production: Techno-economic assessment. Process Safety and Environmental Protection 121, 194–208. https://doi.org/10.1016/j.psep.2018.10.018
40. Leal Silva, J.F., Mariano, A.P., Maciel Filho, R., 2018. Economic potential of 2-methyltetrahydrofuran (MTHF) and ethyl levulinate (EL) produced from hemicelluloses-derived furfural. Biomass and Bioenergy 119, 492–502. https://doi.org/10.1016/j.biombioe.2018.10.008
41. Marianou, A.A., Michailof, C.M., Pineda, A., Iliopoulou, E.F., Triantafyllidis, K.S., Lappas, A.A., 2016. Glucose to Fructose Isomerization in Aqueous Media over Homogeneous and Heterogeneous Catalysts. ChemCatChem 8, 1100–1110. https://doi.org/10.1002/cctc.201501203
42. Mogoș, R.I., Petrescu, I., Chiotan, R.A., Crețu, R.C., Troacă, V.A., Mogoș, P.L., 2023. Greenhouse gas emissions and Green Deal in the European Union. Front. Environ. Sci. 11, 1141473. https://doi.org/10.3389/fenvs.2023.1141473
43. Muralidhara, A., Tosi, P., Mija, A., Sbirrazzuoli, N., Len, C., Engelen, V., De Jong, E., Marlair, G., 2018. Insights on Thermal and Fire Hazards of Humins in Support of Their Sustainable Use in Advanced Biorefineries. ACS Sustainable Chem. Eng. 6, 16692–16701. https://doi.org/10.1021/acssuschemeng.8b03971
44. Ogawa, T., Yoshida, M., Ishihara N., K., 2022. Techno-economic analysis on recent heterogeneous catalysts for ammonia synthesis (preprint). Chemistry. https://doi.org/10.26434/chemrxiv-2022-1vs9p
45. Okolie, J.A., Nanda, S., Dalai, A.K., Kozinski, J.A., 2021. Techno-economic evaluation and sensitivity analysis of a conceptual design for supercritical water gasification of soybean straw to produce hydrogen. Bioresource Technology 331, 125005. https://doi.org/10.1016/j.biortech.2021.125005
46. Peng L, Lin L, Zhang J, Shi J, Liu S. Solid acid catalyzed glucose conversion to ethyl levulinate. Applied Catalysis A: General 2011;397:259–65. https://doi.org/10.1016/j.apcata.2011.03.008
47. Peters, M.S., Timmerhaus, K.D., 1991. Plant Design and Economics for Chemical Engineers, 4th Edition. ed. McGraw Hill - International Editions.
48. Raj, T., Chandrasekhar, K., Banu, R., Yoon, J.-J., Kumar, G., Kim, S.-H., 2021. Synthesis of γ-valerolactone (GVL) and their applications for lignocellulosic deconstruction for sustainable green biorefineries. Fuel 303, 121333. https://doi.org/10.1016/j.fuel.2021.121333
49. Shuai, L., Questell-Santiago, Y.M., Luterbacher, J.S., 2016. A mild biomass pretreatment using γ-valerolactone for concentrated sugar production. Green Chem. 18, 937–943. https://doi.org/10.1039/C5GC02489G
50. Tian, Y., Zhang, F., Wang, J., Cao, L., Han, Q., 2021. A review on solid acid catalysis for sustainable production of levulinic acid and levulinate esters from biomass derivatives. Bioresource Technology 342, 125977. https://doi.org/10.1016/j.biortech.2021.125977
51. Towler, G.P., Sinnott, R.K., 2008. Chemical engineering design: principles, practice and economics of plant and process design. Elsevier/Butterworth-Heinemann, Amsterdam ; Boston.
52. UpCycle, 2019. Livre Blanc - Mettre en place le tri et la valorisation des biodéchets.
53. Van Wortswinkel, L., Nijs, W., 2010. Industrial Combustion Boilers.
54. Villeneuve, J., Palacios, J.H., Savoie, P., Godbout, S., 2012. A critical review of emission standards and regulations regarding biomass combustion in small scale units (<3MW). Bioresource Technology 111, 1–11. https://doi.org/10.1016/j.biortech.2012.02.061

55. Wong, C.Y.Y., Choi, A.W.-T., Lui, M.Y., Fridrich, B., Horváth, A.K., Mika, L.T., Horváth, I.T., 2017. Stability of gamma-valerolactone under neutral, acidic, and basic conditions. Struct Chem 28, 423–429. https://doi.org/10.1007/s11224-016-0887-6
56. W-tech, 2022. Axial Open Type Cooling Tower - datasheet [WWW Document]. URL https://www.w-tech.it/wp-content/uploads/2019/04/TC-TAA-ITA-ENG-R011-MAGNELIS.pdf
57. Zhao D, Wang Y, Delbecq F, Len C. Continuous flow conversion of alkyl levulinates into γ-valerolactone in the presence of Ru/C as catalyst. Molecular Catalysis 2019;475:110456. https://doi.org/10.1016/j.mcat.2019.110456

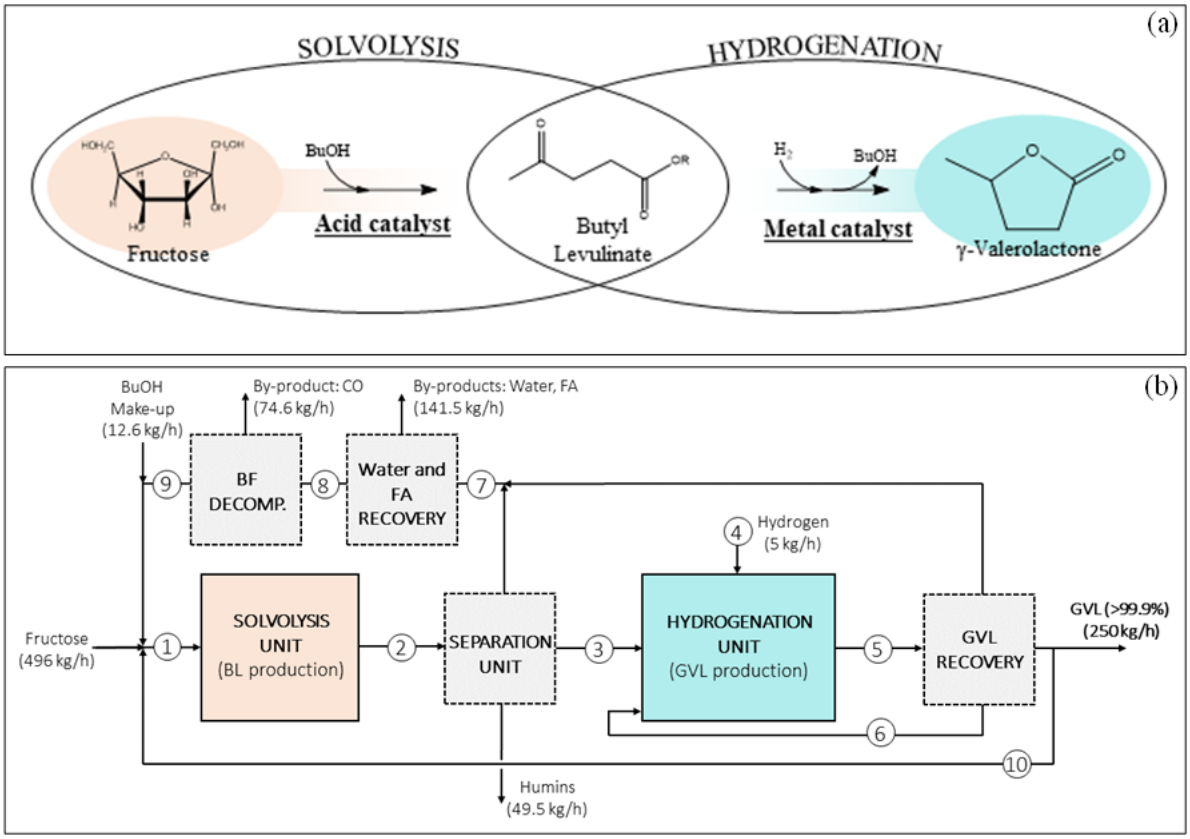

Fig. 1: (a) Chemical route to produce GVL from fructose: (i) acid-solvolysis of fructose to BL; (ii) hydrogenation of BL to GVL. (b) Block Flow Diagram of the production process of GVL from LCB-derived fructose. The mass flow rates of the main streams are reported in kg/h.

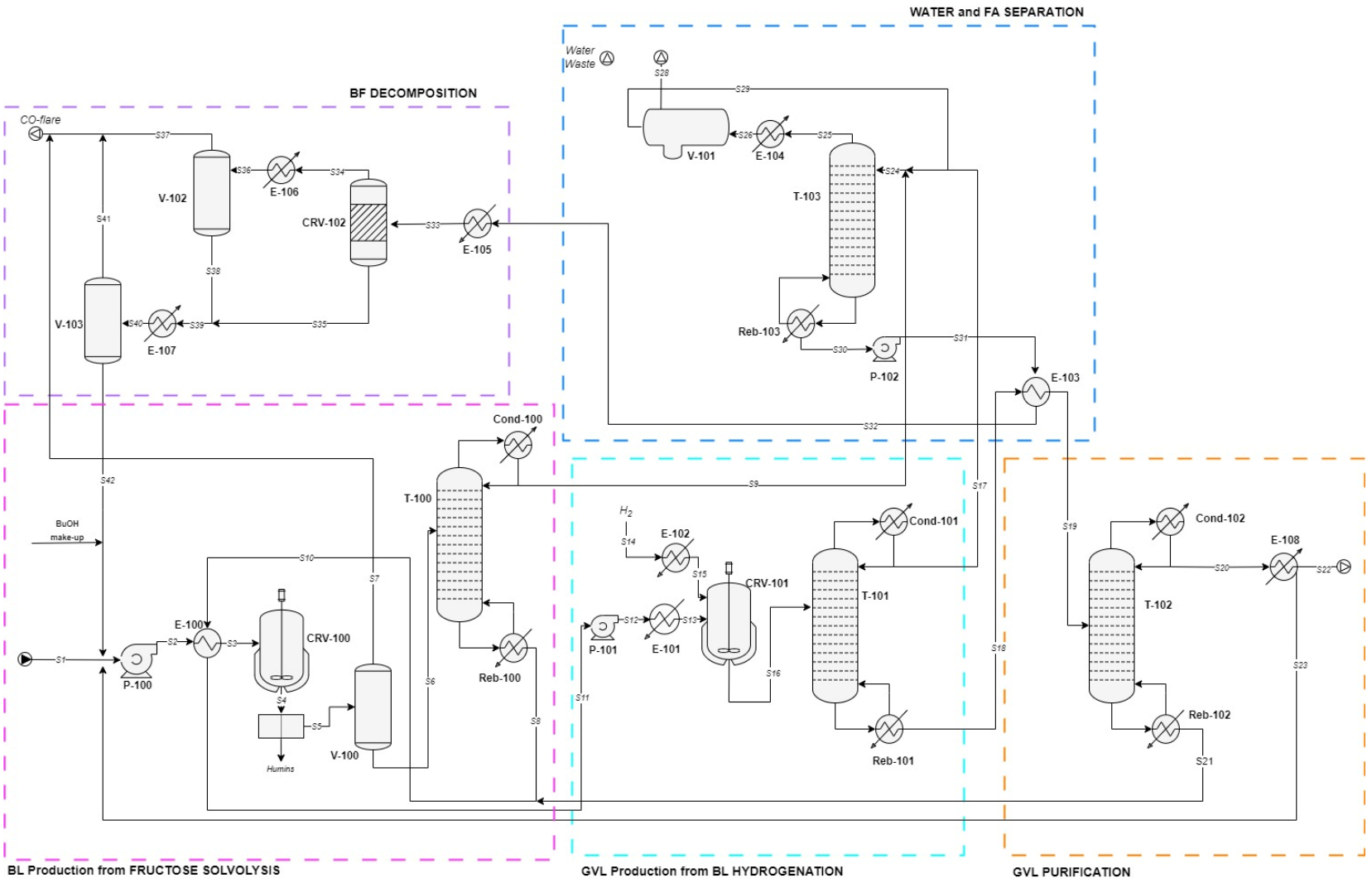

Fig. 2: Preliminary Process Flow Diagram of the designed process for production of GVL from LCB-derived fructose. CRV: Conversion Reactor Vessel. V: Separation Vessel. E: Heat Exchanger between process fluids. P: pump. T: Distillation Column. Reb: reboiler. Cond: condenser.

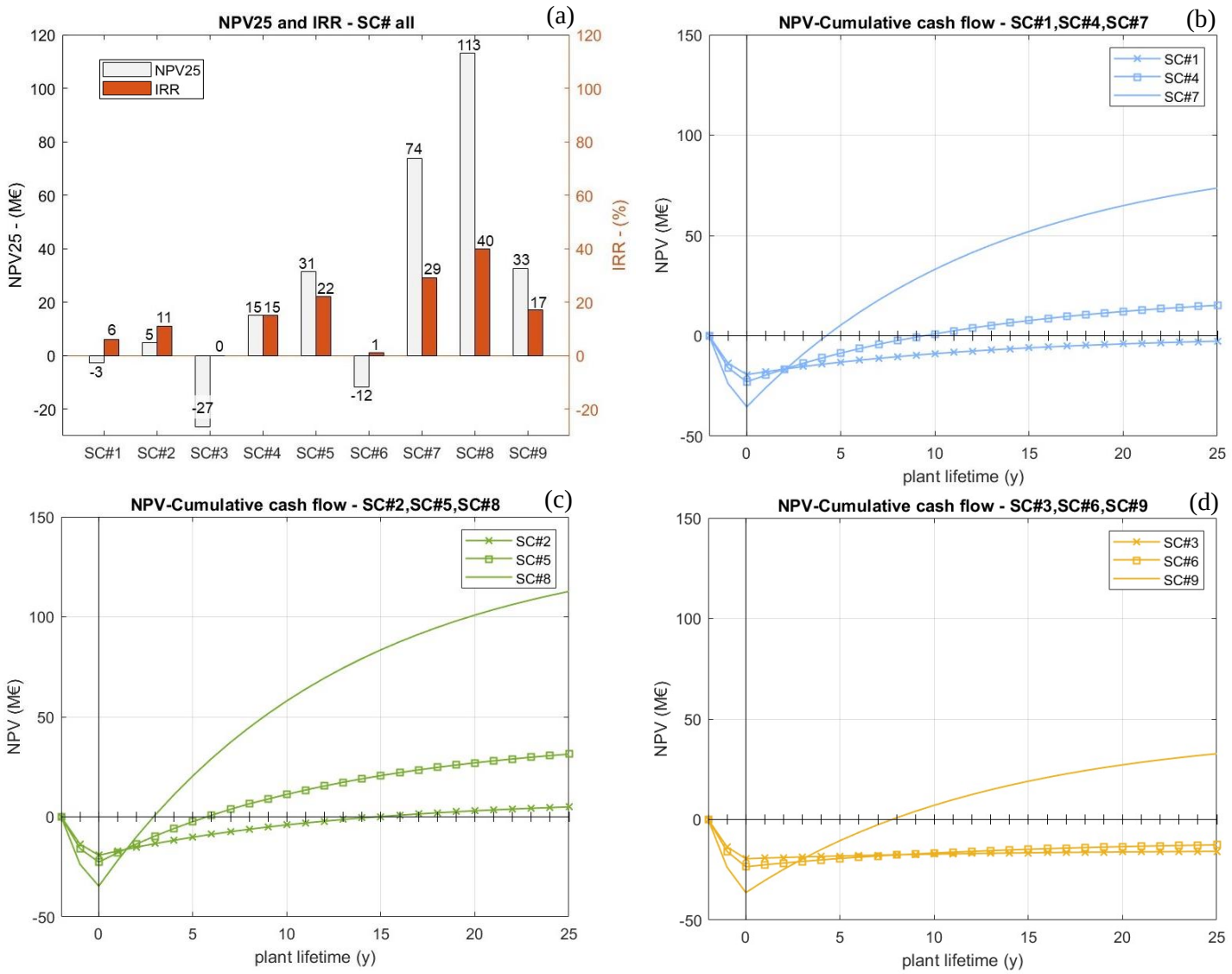

Fig. 3: (a) NPV25 and IRR comparison between scenarios; (b) Cumulative cash flow over the project lifetime for scenarios SC#1-4-7; (c) Cumulative cash flow over the project lifetime for scenarios SC#2-5-8; (d) Cumulative cash flow over the project lifetime for scenarios SC#3-6-9.

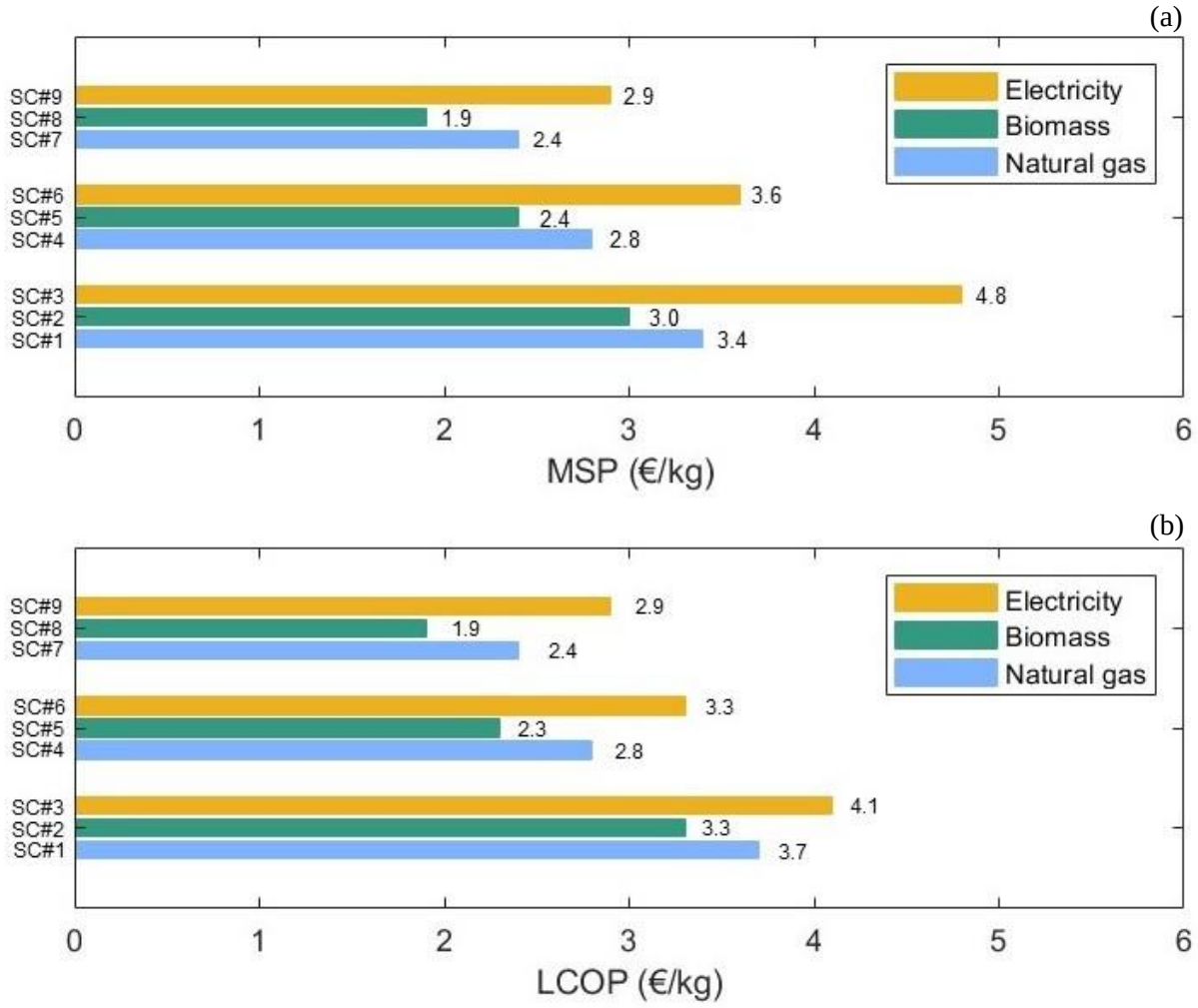

Fig. 4: Minimum selling price (MSP)(a) and LCOP (b) index of the different scenarios.

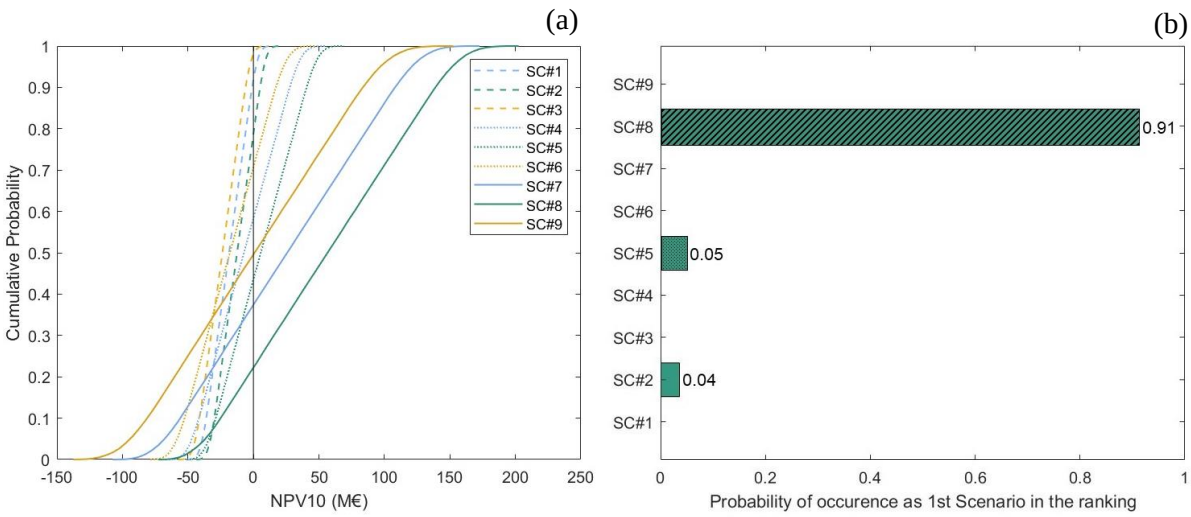

Fig. 5: (a) Cumulative probability trends related to sensitivity and uncertainty analysis on the NPV10;(b) Probability of occurrence as first scenario in terms of NPV10.

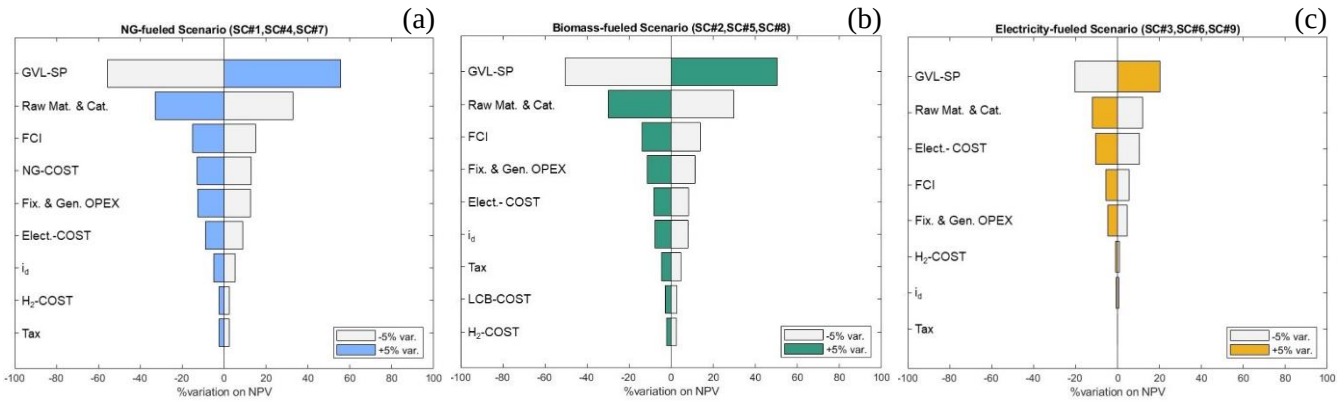

Fig. 6: Influence of key economic variables on the NPV: (a) NG-fueled scenarios; (b) biomass-fueled scenarios; (c) electricity-fueled scenarios.

*Table 1: Properties and conditions of main streams, referred to PFD for the production of GVL from fructose in Fig.2. *: BuOH make-up stream.*

STREAM	1	2	3	4	5	6	7	8	9	10	11	12	13	14	15	16	17	18	19	20	21	Humin
T (°C)	20	39.7	110.0	100.0	99.3	99.3	99.3	238.2	54.4	237.0	127.4	150.0	150.6	20.0	150.0	150.5	28.9	235.9	185.0	205.2	240.8	110.0
P (bar)	1.0	20.1	20.0	20.0	2.0	2.0	2.0	2.2	1.1	2.1	2.0	2.0	20.0	20.0	20.0	2.0	1.1	2.2	1.1	1.1	2.1	20.0
BuOH	0.63	0.63	0.63	0.53	0.54	0.54	0.37	-	0.83	-	-	-	-	-	-	0.12	0.99	-	-	-	-	-
GVL	0.23	0.23	0.23	0.23	0.24	0.24	0.01	0.66	-	0.66	0.66	0.66	0.66	-	-	0.81	-	0.92	0.92	1.00	0.62	-
FRUCT	0.14	0.14	0.14	-	-	-	-	-	-	-	-	-	-	-	-	-	-	-	-	-	-	-
LA	-	-	-	-	-	-	-	-	-	-	-	-	-	-	-	-	-	-	-	-	-	-
FA	-	-	-	-	-	-	-	-	-	-	-	-	-	-	-	-	-	-	-	-	-	-
BL	-	-	-	0.12	0.12	0.12	-	0.33	-	0.27	0.27	0.27	0.27	-	-	-	-	-	-	-	-	-
BF	-	-	-	0.07	0.07	0.07	0.07	-	0.11	-	-	-	-	-	-	-	-	-	-	-	-	-
Water	-	-	-	0.04	0.04	0.04	0.12	-	0.06	-	-	-	-	-	-	-	-	-	-	-	-	-
H_2	-	-	-	-	-	-	-	-	-	-	-	-	-	1.00	1.00	-	-	-	-	-	-	-
BHP	-	-	-	-	-	-	-	-	-	0.07	0.07	0.07	0.07	-	-	0.07	-	0.08	0.08	-	0.38	-
CO	-	-	-	-	-	-	0.43	-	-	-	-	-	-	-	-	-	-	-	-	-	-	-
Humins	-	-	-	0.01	-	-	-	-	-	-	-	-	-	-	-	-	-	-	-	-	-	1.00
Total (kg/h)	3628.7	3628.7	3628.7	3628.7	3579.1	3564.0	15.1	1275.7	2288.4	1547.5	1547.5	1547.5	1547.5	5.0	5.0	1552.5	185.2	1367.4	1367.4	1095.5	271.9	49.5

STREAM	22	23	24	25	26	27	28	29	30	31	32	33	34	35	36	37	38	39	40	41	42	BMU*
T (°C)	20.0	20.0	52.2	95.0	50.0	50.0	50.0	50.0	136.1	137.0	162.9	190.0	190.0	190.0	80.0	80.0	80.0	190.0	19.5	19.5	19.5	20.0
P (bar)	1.0	1.0	1.0	1.1	1.0	1.0	1.0	1.0	2.0	20.7	20.6	20.5	20.5	20.5	20.4	20.4	20.4	20.5	1.0	1.0	1.0	1.0
BuOH	-	-	0.83	0.59	0.59	0.01	0.14	0.75	0.90	0.90	0.90	0.90	0.66	0.99	0.66	0.04	0.98	0.99	0.99	0.03	1.00	1.00
GVL	1.00	1.00	-	-	-	-	-	-	-	-	-	-	-	-	-	-	-	-	-	-	-	-
FRUCT	-	-	-	-	-	-	-	-	-	-	-	-	-	-	-	-	-	-	-	-	-	-
LA	-	-	-	-	-	-	-	-	-	-	-	-	-	-	-	-	-	-	-	-	-	-
FA	-	-	-	0.01	0.01	0.02	0.01	-	-	-	-	-	-	-	-	-	-	-	-	-	-	-
BL	-	-	-	-	-	-	-	-	-	-	-	-	-	-	-	-	-	-	-	-	-	-
BF	-	-	0.11	0.14	0.14	0.03	0.06	0.17	0.10	0.10	0.10	0.10	-	-	-	-	-	-	-	-	-	-
Water	-	-	0.06	0.25	0.25	0.93	0.08	0.07	-	-	-	-	-	-	-	-	-	-	-	-	-	-
H_2	-	-	-	-	-	-	0.01	-	-	-	-	-	-	-	-	-	-	-	-	-	-	-
BHP	-	-	-	-	-	-	0.00	-	-	-	-	-	-	-	-	-	-	-	-	-	-	-
CO	-	-	-	0.01	0.01	0.02	0.69	-	-	-	-	-	0.34	0.01	0.34	0.96	0.02	0.01	0.01	0.97	-	-
Humins	-	-	-	-	-	-	-	-	-	-	-	-	-	-	-	-	-	-	-	-	-	-
Total (kg/h)	250.4	845.1	2992.2	660.6	660.6	141.5	0.4	518.6	2331.5	2331.5	2331.5	2331.5	156.1	2175.4	156.1	53.9	102.2	2175.4	2277.6	5.6	2272.	12.6

Table 2: Heat flow demand of main equipment, referred to PFD for the production of GVL from fructose in Fig.2.

PU	**CRV-100**	**CRV-101**	**CRV-102**	**P-100**	**P-101**	**P-102**	**Cond-100**	**Reb-100**	**Cond-101**	**Reb-101**
Heat flow (10^5 kJ/h)	-15.4	-9.10	1.30	0.10	0.04	0.08	3.23	3.34	2.76	4.94
PU	**Cond-102**	**Reb-102**	**Reb-103**	**E-101**	**E-102**	**E-104**	**E-105**	**E-106**	**E-107**	**E-108**
Heat flow (10^5 kJ/h)	13.7	14.6	11.8	0.08	0.09	7.33	1.96	0.81	9.78	3.96

Table 3: Capital and operative expenses, and assumptions employed in economic indicators analysis.

Assumptions		**References**
Reference year	2022 (8400 working hours)	
Plant lifetime	25 years	(Towler and Sinnott, 2008)
Construction period	2 years	(Towler and Sinnott, 2008)
Working capital	7/8 weeks of operating costs	(Towler and Sinnott, 2008)
Start-up capital	8% of fixed capital investment	(Peters and Timmerhaus, 1991)
Discount rate	8%	(Casson Moreno et al., 2020)
Taxation	20%	(Casson Moreno et al., 2020)
OPEX		
Waste disposal	1.4 €/ton	(Towler and Sinnott, 2008)
N° operator/shift	4 operators per shift	(Towler and Sinnott, 2008)
Labor cost	32€/h – 2080 h/y	(EUROSTAT, 2022)
Maintenance	3% of FCI	(Peters and Timmerhaus, 1991)
Operating supplies	15 % of maintenance cost	(Peters and Timmerhaus, 1991)
Patents and Royalties	1 % of total operating expenses	(Peters and Timmerhaus, 1991)
Overheads	10 % of sum of labor and maintenance	(Towler and Sinnott, 2008)
Local taxes	1 % of FCI	(Peters and Timmerhaus, 1991)
Insurance	1 % of FCI	(Peters and Timmerhaus, 1991)
Administration	25 % of labor cost	(Peters and Timmerhaus, 1991)
Distribution and selling	5 % of operating expenses	(Peters and Timmerhaus, 1991)
Raw materials		
Fructose	€0.7/kg	(Kwan et al., 2019)
Butanol	€1.13/kg	(Baral and Shah, 2016)
GVL	€1.58-4.94/kg	(Byun and Han, 2019)
Hydrogen	€4.75-7.57/kg	(Hydrogen Council, 2020)
Catalysts		
Amberlite IR-120 (H-form)	€60/kg	(Fernández Méndez et al., 2023)
Ru/C	€5.4/g	(Ogawa et al., 2022)
Alumina	€23.5/kg	(Baddour et al., 2018)
DHT-4A	€7.5/kg	(Kisuma Chemicals, 2023)
Utilities		
Electricity	0.127 €/kWh	(EUROSTAT, 2022)
Natural gas	0.073 €/kWh	(EUROSTAT, 2022)
Biomass	0.027 €/kWh	(Kang et al., 2023)
Other utilities		
Chilled water	€0.08/m^3	(Towler and Sinnott, 2008)
Cooling water	€0.03/m^3	(Towler and Sinnott, 2008)
Steam	€0.0145/kg	(Towler and Sinnott, 2008)
Refrigerant fluid (Propane)	1%-Capex Refr.system	(Towler and Sinnott, 2008)

Table 4: CAPEX of the equipment items (from Aspen Process Economic Analyzer).

Equipment item	SIZE-2kt/y		SIZE-4kt/y		SIZE-10kt/y	
	Equip. Cost ($_{2018}$)	**Install. Cost ($_{2018}$)**	**Equip. Cost ($_{2018}$)**	**Install. Cost ($_{2018}$)**	**Equip. Cost ($_{2018}$)**	**Install. Cost ($_{2018}$)**
Reactors	$1.81 \cdot 10^5$	$6.23 \cdot 10^5$	$2.35 \cdot 10^5$	$6.91 \cdot 10^5$	$3.90 \cdot 10^5$	$8.95 \cdot 10^5$
Heat Exchangers	$9.95 \cdot 10^4$	$6.11 \cdot 10^5$	$1.40 \cdot 10^5$	$7.43 \cdot 10^5$	$2.60 \cdot 10^5$	$1.02 \cdot 10^6$
Dist. Columns	$7.44 \cdot 10^5$	$2.27 \cdot 10^6$	$1.28 \cdot 10^6$	$2.99 \cdot 10^6$	$2.79 \cdot 10^6$	$5.22 \cdot 10^6$
Separation. vessels	$7.22 \cdot 10^4$	$4.53 \cdot 10^5$	$7.48 \cdot 10^4$	$4.57 \cdot 10^5$	$8.16 \cdot 10^4$	$4.49 \cdot 10^5$
Pumps	$1.04 \cdot 10^5$	$1.97 \cdot 10^5$	$1.06 \cdot 10^5$	$2.05 \cdot 10^5$	$1.11 \cdot 10^5$	$2.09 \cdot 10^5$
Total Equip. Cost	$1.20 \cdot 10^6$	$4.16 \cdot 10^6$	$1.83 \cdot 10^6$	$5.08 \cdot 10^6$	$3.63 \cdot 10^6$	$7.39 \cdot 10^6$
Including: · Instrumentation (2-8%-TCC) · Piping (3-20%-TCC) · Electrical system (2-10%-TCC) · Building (3-18%-TCC) · Yard improv. (2-5%)				· Services (8-20%-TCC) · Land (1-2%-TCC) · Engineering (4-21%-TCC) · Construction (4-16%-TCC) · Contractor's fees (2-6%-TCC) · Contingency (5-15%-TCC)		
Total Capital Cost-TCC ($-2018)	$10.6 \cdot 10^6$		$12 \cdot 10^6$		$14.7 \cdot 10^6$	
Total Capital Cost-TCC (€-2022)	$15.5 \cdot 10^6$		$17.4 \cdot 10^6$		$21.5 \cdot 10^6$	

Table 5: Energy and utilities requirements for scenarios.

Production scale [kt/year]	**Power demand [MW]**	**Heat demand [MW]**	**Thermal Energy Supply Scenario**		
			Natural gas [m^3/h]	**Biomass [kg/h]**	**Electricity [MWh]**
2	0.78	1.92	460 (SC#1)	355 (SC#2)	1.92 (SC#3)
4	1.85	3.92	939 (SC#4)	728 (SC#5)	3.92 (SC#6)
10	3.84	9.27	2220 (SC#7)	1718 (SC#8)	9.27 (SC#9)

Table 6: Capital and operating expenses for each scenario.

Energy Scenario	2 kt/y SC#1	SC#2	SC#3	4 kt/y SC#4	SC#5	SC#6	10 kt/y SC#7	SC#8	SC#9
FCI (10^6 €)	17	17	17	19.8	19.8	19.8	29.7	29.7	29.7
Working capital (10^6 €)	1.0	0.8	1.1	1.6	1.3	2.1	3.4	2.6	4.3
Start-up capital (10^6 €)	1.4	1.4	1.4	1.6	1.6	1.6	2.4	2.4	2.4
Total investment (10^6 €)	19.4	19.2	19.5	23	22.7	23.5	35.5	34.7	36.4
OPEX									
Variable operating expenses (10^6 €/y)									
Raw material	3.56	3.56	3.56	7.16	7.16	7.16	17.0	17.0	17.0
Catalyst	0.01	0.01	0.01	0.02	0.02	0.02	0.03	0.03	0.03
Utilities	2.07	1.44	3.03	3.99	2.67	6.24	10.4	7.20	15.8
Waste treatment	-2.45	-2.65	-2.45	-4.85	-5.27	-4.85	-11.6	-12.7	-11.6
Fixed operating expenses (10^6 €/y)									
Operating labor	1.04	1.04	1.04	1.04	1.04	1.04	1.04	1.04	1.04
Maintenance	0.51	0.51	0.51	0.59	0.59	0.59	0.89	0.89	0.89
Operating supplies	0.08	0.08	0.08	0.09	0.09	0.09	0.13	0.13	0.13
Patents-royalties	0.06	0.05	0.07	0.09	0.09	0.12	0.20	0.16	0.26
Overheads	0.16	0.16	0.16	0.16	0.16	0.16	0.19	0.19	0.19
Local taxes	0.17	0.17	0.17	0.20	0.20	0.20	0.30	0.30	0.30
Insurance	0.17	0.17	0.17	0.20	0.20	0.20	0.30	0.30	0.30
General operating expenses (10^6 €/y)									
Administration	0.26	0.26	0.26	0.26	0.26	0.26	0.26	0.26	0.26
Logistic	0.30	0.25	0.35	0.47	0.38	0.59	1.01	0.78	1.29
Annual operating costs (10^6 €/y)	5.95	5.05	6.95	9.42	7.57	11.8	20.1	15.6	25.9